International Journal of Nanomedicine

Dovepress
Taylor & Francis Group

Open Access Full Text Article

ORIGINAL RESEARCH

Inhibition of Ferroptosis by Adipose Stem Cell-Derived Apoptotic Vesicles Enhances Angiogenesis and Accelerates Diabetic Wound Healing

Jingyi Zhang[1,2,*], Jinxin Kuang[1,*], Shengkai Gong[1,3,*], Hanzhe Wang[1], Feng Ding[1,3], Lu Zhao[1,4], Lele Shi[1,4], Shiyu Liu[1,3], Yimin Zhao[1], Jiani Liu[1,5], Geng Dou[1,3]

[1]State Key Laboratory of Oral & Maxillofacial Reconstruction and Regeneration, National Clinical Research Center for Oral Diseases, School of Stomatology, The Fourth Military Medical University, Xi'an, Shaanxi, 710032, People's Republic of China; [2]School of Basic Medicine, The Fourth Military Medical University, Xi'an, Shaanxi, 710032, People's Republic of China; [3]State Key Laboratory of Oral & Maxillofacial Reconstruction and Regeneration, National Clinical Research Center for Oral Diseases, Shaanxi Key Laboratory of Stomatology, Department of Oral Biology & Clinic of Oral Rare Diseases and Genetic Disease, School of Stomatology, the Fourth Military Medical University, Xi'an, Shaanxi, 710032, People's Republic of China; [4]State Key Laboratory of Oral & Maxillofacial Reconstruction and Regeneration, National Clinical Research Center for Oral Diseases, Shaanxi Clinical Research Center for Oral Diseases, Department of Oral and Maxillofacial Surgery, School of Stomatology, The Fourth Military Medical University, Xi'an, Shaanxi, 710032, People's Republic of China; [5]State Key Laboratory of Oral & Maxillofacial Reconstruction and Regeneration, National Clinical Research Center for Oral Diseases, Shaanxi Key Laboratory of Stomatology, Digital Center, School of Stomatology, The Fourth Military Medical University, Xi'an, Shaanxi, 710032, People's Republic of China

*These authors contributed equally to this work

Correspondence: Geng Dou, State Key Laboratory of Oral & Maxillofacial Reconstruction and Regeneration, National Clinical Research Center for Oral Diseases, School of Stomatology, The Fourth Military Medical University, No. 145, West Changle Road, Xi'an, Province Shaanxi, 710032, People's Republic of China, Email doug0714@163.com; Jiani Liu, State Key Laboratory of Oral & Maxillofacial Reconstruction and Regeneration, National Clinical Research Center for Oral Diseases, Shaanxi Key Laboratory of Stomatology, Digital Center, School of Stomatology, The Fourth Military Medical University, No. 145, West Changle Road, Xi'an, Province Shaanxi, 710032, People's Republic of China, Email jenny170219@163.com

Purpose: Impaired angiogenesis is a critical challenge in diabetic wound healing. While apoptotic derivatives of stem cells hold promise for regenerative therapy, their role in modulating angiogenesis within the diabetic wound microenvironment remains underexplored. This study aims to investigate whether adipose stem cell-derived apoptotic vesicles (ASCs-apoVs) promote angiogenesis and accelerate diabetic wound healing by inhibiting endothelial cell ferroptosis.

Methods: Diabetic mice model was established by feeding with high-fat diet (HFD) for 3 months followed by full-thickness skin wound preparation. Adipose stem cells (ASCs) isolated from adipose tissue were treated with staurosporine (STS) to induce apoptosis in vitro. Apoptotic vesicles (apoVs) were isolated by differential centrifugation, characterized using TEM, dynamic light scattering (DLS), and Western blot, and applied topically to diabetic wounds. The therapeutic effects of apoVs on wound healing efficiency, vascularization level and endothelial cell ferroptosis were evaluated.

Results: HFD-induced diabetes promoted lipid peroxidation (4HNE accumulation) and ferroptosis in endothelial cells (ECs), leading to reduced $CD31^+$ and vWf^+ vessel density and delayed wound closure. In vitro diabetic endothelial cell models confirmed increased lipid peroxidation and ferroptosis, which compromised the proliferation, migration and tube formation capacities of ECs. ASCs-apoVs, characterized by typical extracellular vesicle (EV) morphology and apoptotic markers, significantly inhibited lipid peroxidation and ferroptosis of ECs, thereby promoting angiogenesis and accelerating diabetic wound healing.

Conclusion: Ferroptosis of endothelial cells contributes to impaired vascularization in diabetic wounds. ApoVs represent a promising cell-free therapeutic approach to mitigate ferroptosis, restore endothelial function and promote angiogenesis, offering a potential strategy for diabetic wound management.

Keywords: apoptotic vesicles, wound healing, vascularization, adipose stem cells, ferroptosis, endothelial cells

Received: 26 March 2025
Accepted: 26 July 2025
Published: 6 August 2025

Introduction

Skin functions as the body's primary defense against external stimuli, performing essential roles in maintaining homeostasis, regulating body temperature, and facilitating metabolic processes.[1,2] Skin injuries arise not only from trauma but also as manifestations of various pathological conditions, including inflammation, neoplasia, and autoimmune disorders.[3,4] Diabetes mellitus, a prevalent metabolic disease caused by excess nutrition intake, significantly impairs the skin's capacity for repair post-injury.[5,6] This impairment adversely affects patients' quality of life and imposes substantial demands on healthcare resources due to prolonged treatment durations and elevated medical expenses. Despite extensive research, the precise mechanisms by which diabetes disrupts the wound healing process remain insufficiently elucidated. Angiogenesis, the formation of new blood vessels, is an indispensable step deeply involved in the dynamic balance of the wound microenvironment, ensuring an adequate supply of oxygen and nutrients, thus enabling effective repair.[7–10] Current therapeutic strategies, such as the clinical application of cytokines like vascular endothelial growth factor (VEGF), encounter challenges including translational hurdles, stability issues, and cost considerations, thereby restricting their efficacy.[11,12] Consequently, investigating the underlying mechanisms of angiogenesis impairment in diabetic conditions is imperative for developing more targeted and effective interventions.

The repair process after injury is complicated by the metabolic disturbances of diabetes. Diabetes affects the health and homeostasis of various tissues through diverse metabolic pathways, giving rise to complications such as diabetic neurodegeneration, periodontitis, and retinopathy.[13–15] Refractory diabetic wounds, a severe complication of diabetes, characterized by prolonged non-healing, recurrent infections, and impaired angiogenesis, pose a significant clinical challenge due to persistent inflammation, abnormal microvasculature, and the diabetic microenvironment's inhibitory effects on cell proliferation and migration.[16] Given the vascular system's unique anatomical proximity to the circulatory system, diabetes-induced metabolic perturbations inflict varying degrees of damage on the vascular system.[17,18] Diabetes-induced metabolic perturbations, particularly lipid peroxidation, promote ferroptosis, a new type of cell death linked to β-cell dysfunction, insulin resistance, and diabetic cardiomyopathy.[19–21] Dyslipidemia exacerbates intracellular lipid peroxide accumulation, creating a permissive environment for ferroptosis and microcirculatory damage.[22,23] Clarifying the role of ferroptosis in this context holds promise for therapeutic innovation.

Mesenchymal stem cells (MSCs), as progenitor cells residing in interstitial tissues (eg, adipose tissue, bone marrow, dental pulp) with potent proliferative capacity and multi-lineage differentiation potential, have emerged as pivotal players in regenerative medicine.[24–27] Despite numerous approved MSCs-related clinical trials, frustratingly few have translated into effective therapies,[25,28] hampered by challenges in cell source quality control, biological heterogeneity, insufficient safety/efficacy verification, the high costs and regulatory gaps that demand urgent resolution.[25,29] The development of cell-free therapies, such as stem cell-derived apoptotic vesicles (apoVs), emerge as a viable alternative.[30,31] Our previous research demonstrated that transplanted stem cells generated therapeutic effect through apoVs.[32,33] ApoVs, a special type of vesicles released by cells during apoptosis, feature low immunogenicity, superior stability, and enhanced delivery efficiency, enabling targeted microenvironment modulation for tissue repair.[34–36] These vesicles, historically referred to as apoptotic bodies (ABs)[37] or apoptotic extracellular vesicles (apoEVs),[38,39] encapsulate a diverse cargo of bioactive molecules that actively promote tissue repair by stimulating angiogenesis, mitigating inflammation, and enhancing cell survival.[40] Apoptotic metabolites also actively regulated the gene expression patterns of adjacent cells to restore physiological homeostasis.[41] Leveraging these unique properties, apoVs represent a compelling strategy to overcome the limitations of current therapies and advance the treatment of diabetic wounds.

This study aims to investigate the role of ferroptosis in impaired angiogenesis during diabetic wound healing. We seek to explore whether ASC-apoVs can target metabolic stress-induced lipid peroxidation to alleviate endothelial cell ferroptosis and promote angiogenesis in diabetic wounds. By dissecting the link between metabolic stress, ferroptosis, and vascular dysfunction, this research may establish ASC-apoVs as a novel cell-free therapy for diabetic wound healing.

Materials and Methods

Cell Culture

Adipose stem cells (ASCs) were isolated from murine subcutaneous adipose tissue. The adipose tissue was excised from the subcutaneous area of the groin and rinsed with cold PBS for 3 times. Then, the adipose tissue was cut into small

pieces (2mm×2mm×2mm) and was resuspended with collagenase I (LS004194, Worthington) for digestion under shaking at 37°C (1h). After filtration with a 100-μm filter, the suspension was centrifuged (1200 rpm, 5 min) to concentrate the cells for culture with α-MEM medium supplemented with 10% fetal bovine serum (FBS) and 1% penicillin/streptomycin. Passage 2–3 was used for all experiments in this study. Stem cell surface markers were identified by flow cytometry. The isolated cells were incubated in dark at 37°C for 30 min with PE-conjugated anti-mouse CD73 (127205, BioLegend), anti-CD90 (166408, BioLegend), anti-CD45 (147711, BioLegend), anti-CD11b (101208, BioLegend) and FITC-conjugated anti-mouse anti-CD105 (MA5-17945, eBioscience), respectively. After washing with PBS for 2 times, the cells were detected by the flow cytometer (Beckman Coulter, USA).

For colony-forming unit assay, ASCs were seeded in 96-well plate at a density of 5×10^2 cells/well and cultured in medium for 1–2 weeks. The photograph of colony was taken by using an inverted optical microscope (Olympus, Japan). For osteogenic/adipogenic differentiation, ASCs were seeded in 6-well plate at a density of 6×10^5 cells/well, and incubated with osteogenic/adipogenic induction medium. After 3 weeks of osteogenic induction, Alizarin red staining was conducted (G1038, Servicebio). After 1 week of adipogenic induction, Oil Red O staining was conducted (G1015, Servicebio). Photograph was taken by an inverted optical microscope (Olympus, Japan). Osteogenic induction medium: α-MEM containing 10% FBS, 1% penicillin/streptomycin, 5 mM β-glycerophosphate, 50 μg/mL ascorbic acid, and 10 nM dexamethasone (Sigma-Aldrich, USA). Adipogenic induction medium: α-MEM containing 10% FBS, 0.5 mM isobutylmethylxanthine, 0.5 mM dexamethasone, and 60 nM indomethacin (Sigma-Aldrich, USA).

HUVECs were purchased from FuHeng corporation (FH1122) and maintained in Endothelial Cell Medium (1001, ScienCell, USA) supplemented with 10% FBS and 1% penicillin/streptomycin.

All cells were incubated at 37°C in a humidified atmosphere with 5% CO_2 (Thermo Fisher Scientific).

Animals and Establishment of Diabetic Mice Model

C57BL/6J mice were obtained from Animal center of the Fourth Military Medical University. All mice were maintained under specific pathogen-free conditions with a 12-h light/dark cycle. All mice were kept feeding and drinking ad libitum. Animal experiments in this study were approved and performed in accordance with the Guidelines of Institutional Animal Care Committee of the Fourth Military Medical University.

Diabetic mouse models were constructed by feeding a high-fat diet (HFD) (60% kcal from fat; HF60, Dyets) from six weeks of age for at least 3 months. Mice of the same age were fed a normal chow diet were served as controls. Then, the body weight and blood glucose level of the mice in both groups were measured over 2 weeks. For intraperitoneal glucose tolerance test (IPGTT), mice were fasted for 16 h and intraperitoneally injected with D-glucose (2 g/kg body weight) (HY-B0389, MCE). Blood glucose levels were measured using a glucometer (Roche, Germany) at 0, 15, 30, 60, 90 and 120 min after D-glucose administration. Livers were collected for further histological analysis.

Establishment of Wound Healing Model and Treatment

Wound healing model was established by generating a full-thickness round wound with the diameter of 10 mm in the back of Ctrl or HFD mice. The wound size was recorded on days 0, 5, 10 and 15 post-wounding and calculated with Image J. For the apoVs treatment, apoVs solution (200 μg by protein measurement) was injected subcutaneously around the wound region for 3 times at D3/6/9. At D15, the healing tissue around wound region were harvested for further investigation.

Histological Analysis

The liver and skin samples were fixed, dehydrated and embedded for preparation of sections. The liver sections were performed the H&E (GP1031, Servicebio), Oil red O (GP1067, Servicebio), Sirius red (GP1033, Servicebio) and Nile Red (60530ES03, YEASEN) staining according to the instruction. The skin sections were performed the H&E (GP1031, Servicebio) and Masson (GP1032, Servicebio) staining according to the instruction. The images were captured by Olympus workstation and analyzed by Image J.

Isolation and Characterization of Apoptotic Vesicles

ASCs were treated with staurosporine (sts, 0.5μM) (#9953S, Cell signaling technology) for 4 h to induce apoptosis. Then, the supernatants were collected and centrifuged at 800 g for 10 min to remove the cell debris. Apoptotic vesicles (apoVs) were obtained by centrifugation at 16000 g for 30 min. The generated apoVs were resuspended in PBS and were quantified by BCA method (GK10009, GlpBio). The morphology of apoVs was determined by transmission electron microscope (TEM, TECNAI Spirit, FEI). Annexin V staining was performed using an apoptosis assay kit (40302ES, YEASEN). The size distribution of apoVs was measured by DLS analysis using a Zetasizer Nano ZSE (Malvern, UK).

Detection of Endothelial Cell Ferroptosis

The diabetic endothelial cell model was established by coincubation of HFD mice plasma extracellular vesicles (HEVs) with HUVECs. HUVECs treated with control mice plasma extracellular vesicles (CEVs) were served as negative control. CEVs and HEVs were isolated from plasma by sequential centrifugation (2000 g for 10 min, 10,000 g for 10 min) to remove cell debris and ultracentrifugation at 100,000 g for 12 h (Beckman, USA) to pellet the EVs. The EVs pellet was resuspended in PBS and filtered through a 0.22-μm membrane to remove contaminants. EVs were quantified using the BCA assay (GK10009, GlpBio) and administrated into HUVECs medium at 50 μg/mL for 24 h. The morphology and size of CEVs and HEVs was determined by TEM (TECNAI Spirit, FEI) and Nano Flow Cytometry (Flow NanoAnalyzer, NanoFCM). Ferrostatin-1 (Fer-1) was used as the inhibitor of ferroptosis at 2 μM (HY-100579, MedChemExpress). Ferroptosis level of HUVECs were identified by cell viability, reactive oxygen species (ROS) level, and lipid peroxidation levels. The effect of apoVs were investigated by treatment of HEVs-treated HUVECs with apoVs (50 μg/mL) for 24 h.

After different treatments, cell viability of HUVECs was detected by CCK8 kit (40203ES, YEASEN). The ROS level was measured by fluorescence imaging of cytoplasmic ROS (DCFH-DA, S0033S, Beyotime) and mitochondrial ROS (mitoSOX, 40778ES, YEASEN). Lipid peroxidation levels were identified by staining with C11-BODIPY (GC40165, Glpbio). The cells were collected for flow cytometry to separate the oxidated population.

Immunofluorescence

The tissue was prepared into 10-μm frozen section. After washing with PBS to remove the embedding medium, the tissues were permeated with 0.1% Triton X-100 for 15 min. Then, the sections were blocked with goat serum for 30 min at 37°C. Subsequently, the sections were incubated with the primary antibody (1:200) at 4°C overnight. After washing with PBS for 3 times, the sections were incubated with the fluorescence-conjugated secondary antibodies for 1 h at 37°C. Finally, the sections were counterstained with DAPI and imaged with confocal microscope (Nikon A1+, Japan). The steps of immunofluorescence in cell samples are basically the same as above.

The primary antibodies include: CD31 (ab222783, Abcam), vWf (GB11020, Servicebio), cytokeratin 14 (CK14, ab181595, Abcam), Collagen 3 (GB111629, Servicebio), 4HNE (ab48506, Abcam), Ki67 (ab16667, Abcam). The secondary antibodies include: YSFluor™ 488 Goat Anti-Rabbit lgG (H+L) (33106ES, YEASEN), YSFluor™594 Rabbit Anti-Mouse lgG (H+L) (33912ES, YEASEN). The dye kits include: DiI probe (40726ES, YEASEN), TUNEL cell apoptosis detection kit (C1086, Beyotime), iFluor™ 488 phalloidin (40736ES, YEASEN).

Western Blotting

Western blotting was performed to identify the protein constitution of CEVs, HEVs or apoptotic ASCs. The protein samples from ASCs, apoptotic ASCs, CEVs and HEVs were prepared and performed the SDS-PAGE. The proteins in the gel were transferred to polyvinylidene difluoride (PVDF) membranes. After blocking with 5% bovine serum albumin (BSA) solution, PVDF membranes were incubated with primary antibodies (caspase-3, CD63, Alix, TSG101, Calnexin and GAPDH) at 4°C overnight. Then, PVDF membranes were incubated with the secondary antibodies for 1 hour. Films were developed using Western ECL chemiluminescent kit (AP0082S, AccuRef Scientific) with an imaging system (Tanon 4600, Shanghai). The antibodies used in this study included: caspase-3 (#9662, Cell Signaling Technology), CD63 (sc-5275, Santa Cruz Biotechnology), Alix (#92880, Cell Signaling Technology), TSG101 (#72312, Cell Signaling

Technology), Calnexin (ab22595, Abcam) and GAPDH (30201ES20, YEASEN), HRP-conjugated anti-rabbit secondary antibody (A0208, Beyotime), HRP-conjugated anti-mouse secondary antibody (A0216, Beyotime).

Cell Scratch Assay

HUVECs were seeded in 6-well plate at a density of 6×10^5 cells/well. After 12 h, the scratch was made on the plates by using 1-mL sterile pipette tips. After refreshing the medium, different treatments (the same protocol with *Detection of endothelial cell ferroptosis*) were administrated until the end of the experiment. Photographs were recorded at 0 h, 8 h and 24 h. The area of scratch and wound closure rate were calculated by Image J software.

Tube Formation Assay

80 μL matrigel (354234, Corning) was plated on the 96-well plate and was incubated at 37°C for 30 min. HUVECs in different groups were collected and seeded in the plate at a density of 4×10^4 cells/well. After incubation for 4 h, the photographs were captured and angiogenesis analysis was performed by Image J software.

Statistical Analysis

All data are presented as mean ± standard deviation (s.d). For the statistical analysis, a two-tailed Student's *t*-test was employed when comparing two groups. When analyzing data from more than two groups, one-way analysis of variance (ANOVA) was utilized. For post-hoc analysis, Tukey's test was applied when the variances were homogeneous, while Dunnett's T3 test was used when the variances were not homogeneous. P values less than 0.05 were considered statistically significant. The statistical analyses were performed using SPSS software version 22.0 (IBM, USA). Graph analysis was performed using GraphPad Prism 9.00 (GraphPad Software, USA).

Results

Impaired Vascularization Contributed to Inferior Wound Healing in the Diabetic Model

Six-week-old wild-type mice were fed a high-fat diet (HFD) or a standard chow diet to establish a diabetic mice model and age-matched controls, respectively (Figure 1A). After three months, HFD induced a significant increase in the body size and weight of the mice (Figure 1B and C). Quantitative blood glucose measurement showed significantly elevated levels (>18 mmol/L) in the HFD group compared to Ctrl group (Figure 1D). To further assess glucose homeostasis, an intraperitoneal glucose tolerance test (IPGTT) was performed (Figure 1E). Following a 16-hour fast, fasting blood glucose levels were significantly higher in the HFD group (7.6 mmol/L, 253.08 mg/dL) compared to Ctrl group (4.73 mmol/L, 157.62 mg/dL). Intraperitoneal glucose administration resulted in a rapid increase in blood glucose to 25 mmol/L (832.5 mg/dl) within 30 minutes. The rate of subsequent blood glucose recovery was significantly slower in the HFD group, indicating impaired glucose tolerance. The area under the curve (AUC) for the IPGTT in the HFD group was significantly greater than that in the Ctrl group (Figure 1F). Furthermore, liver tissue was collected for histological analysis, given its established role in hyperglycemia-associated pathology. Hematoxylin-eosin (H&E) and Sirius red staining revealed no evidence of hepatic fibrosis in either group (Figure 1G). However, HFD mice exhibited numerous vacuolar changes in the liver tissue. Oil Red O staining confirmed significant hepatic steatosis (Figure 1H). Nile red staining further supported the presence of increased hepatic neutral lipids. These findings collectively demonstrated the successful induction of a diabetic phenotype in the HFD group.

On this basis, skin wounds were prepared on these HFD mice and Ctrl mice, and the natural healing process without any treatment was observed. The evaluation of the healing process showed that wound closure was significantly slower in the HFD mice compared to Ctrl mice (Figure 1I and J). Statistical analysis of the wound closure rate at day 5 (D5) revealed a significantly lower closure rate (37.67%) in the HFD group compared to Ctrl group (54.87%). This difference persisted at day 10 [D10; 70.03% (HFD) vs 79.32% (Ctrl)]. By day 15 (D15), skin wounds were essentially fully closed in the Ctrl group, while 5% of the wounds in the HFD group remained unhealed. These quantitative analyses firmly

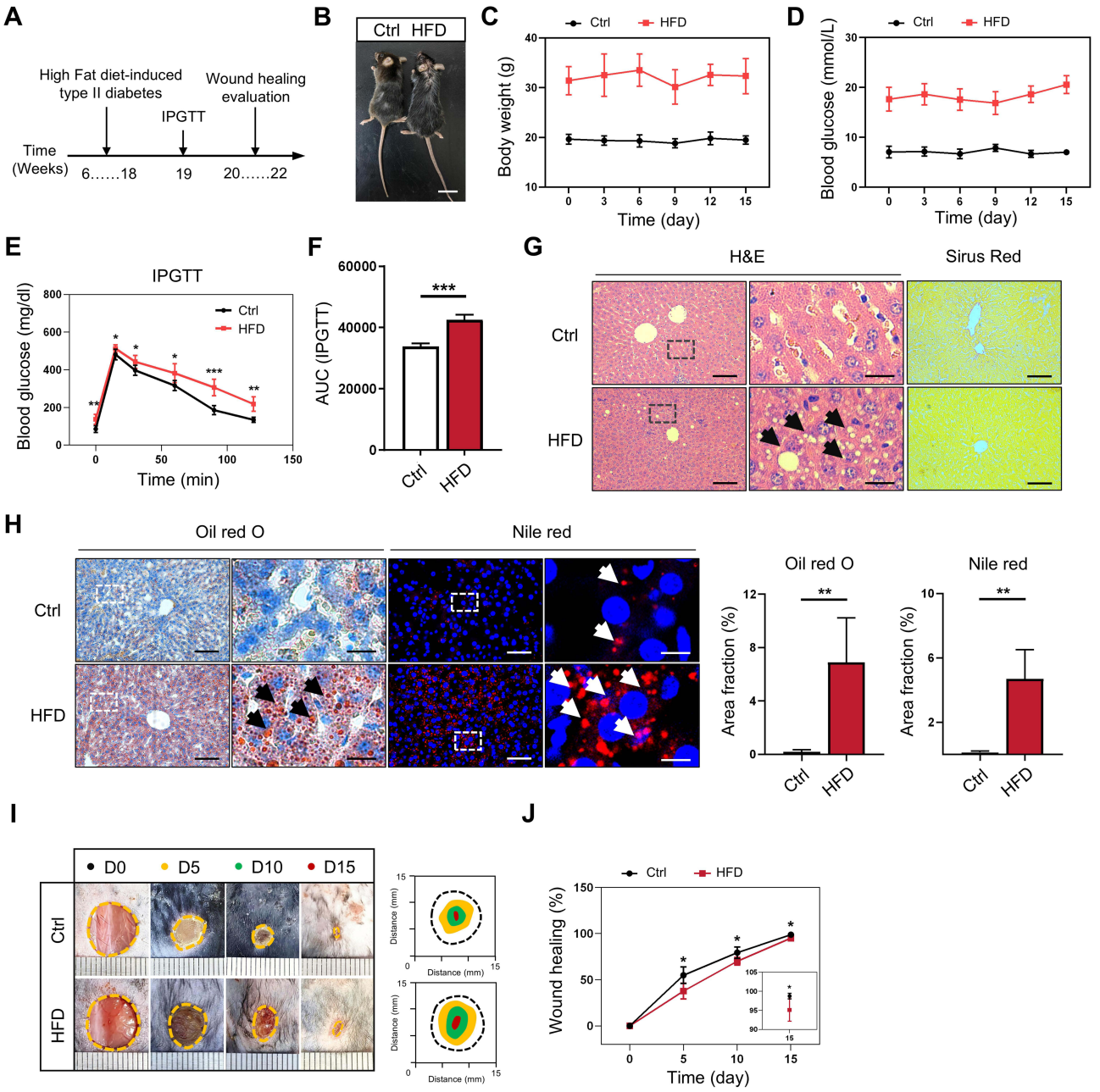

Figure 1 Delayed skin wound healing in diabetic mice model. (**A**) Diagram showed the establishment of high-fat diet (HFD)-induced diabetic wound healing model. (**B**) Photo of control (Ctrl) mice and HFD mice. Scale bar, 2 cm. (**C** and **D**) Body weight and blood glucose level of Ctrl mice and HFD mice. (**E** and **F**) Blood glucose levels during IPGTT and quantification of area under the curve (AUC). (**G**) H&E and Sirius red staining of liver from Ctrl mice and HFD mice. Scale bar, 100 μm (low magnification) and 20 μm (high magnification). (**H**) Oil red O and Nile red staining of liver from Ctrl mice and HFD mice. Scale bar, 100 μm (low magnification) and 20 μm (high magnification) for Oil red O, 50 μm (low magnification) and 10 μm (high magnification) for Nile red. (**I** and **J**) Representative photographs of skin wounds and quantitative analysis of the wound healing rate in each group. *p < 0.05, **p < 0.01 and ***p < 0.001 by student's t test.

indicate the wound healing impairment in diabetic mice, evidenced by the significance at three observation timepoints (Figure 1J; D5, p*=0.014; D10, p*=0.023; D15, p*=0.028).

Diabetes Impaired Angiogenesis During Wound Healing by Inducing ECs Ferroptosis

In order to further investigate the biological process of skin wound healing, we first studied and compared the structure and vascularization level of normal skin in Ctrl and HFD mice. In general, H&E and Masson staining revealed no significant difference in overall skin structure between HFD mice and Ctrl mice (Figure 2A). However, HFD mice

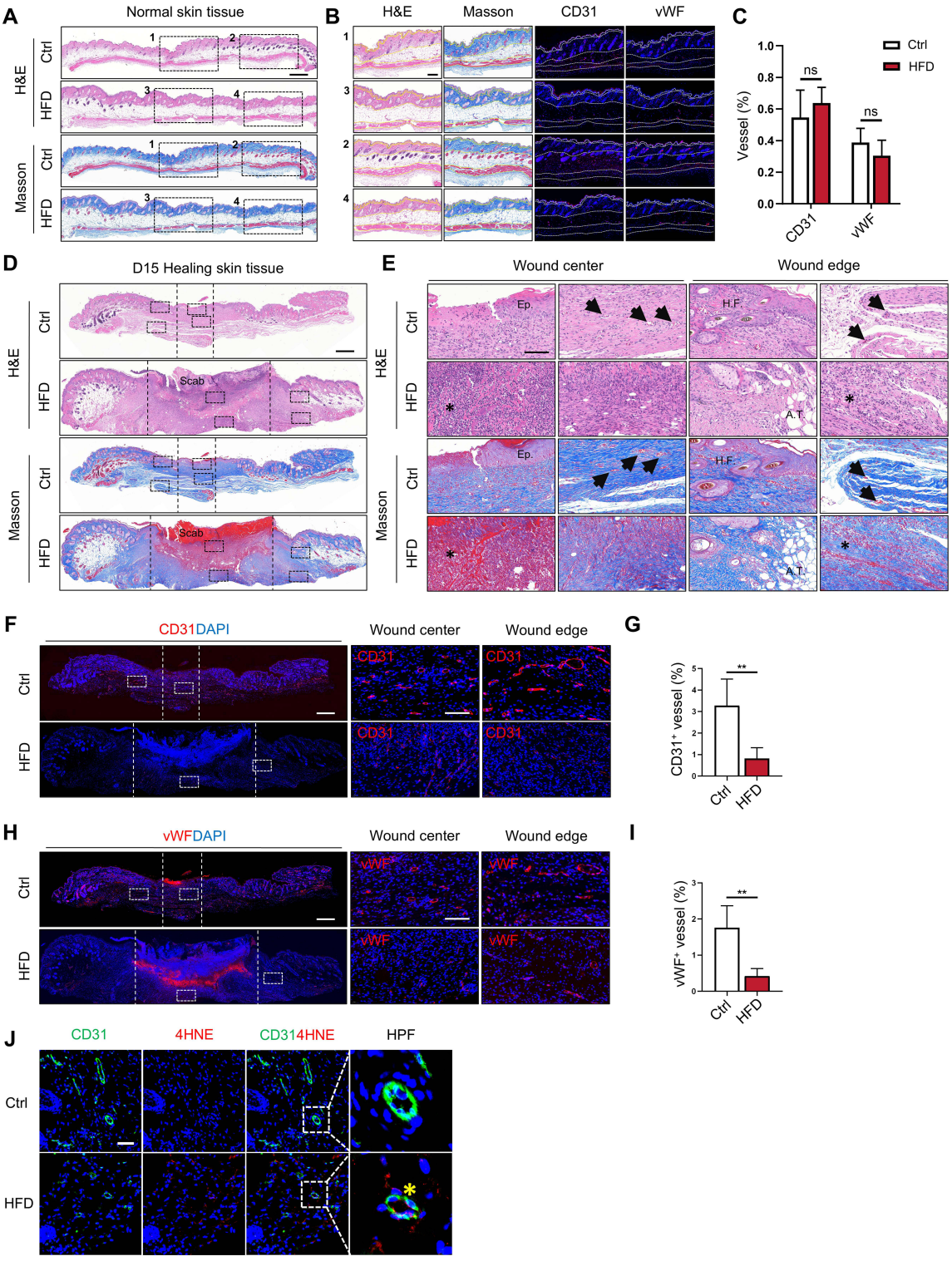

Figure 2 Ferroptosis of endothelial cells resulted in impaired vascularization of diabetic wound. (**A**) H&E and Masson staining of normal skin tissue from Ctrl mice and HFD mice. Scale bar, 500 μm. (**B**) The high-magnified images of the box area (**A**) in normal skin by H&E, Masson, CD31 and vWF staining. Scale bar, 200 μm. (**C**) Quantification of $CD31^+$ or vWF^+ vessel area (% total area) in the normal skin. (**D** and **E**) H&E and Masson staining of the wounded skin from Ctrl mice and HFD mice at D15. The high-magnified images of the dotted box area in the center and edge of the wound (**D**) are shown in (**E**). Scale bar, 500 μm (**D**) and 100 μm (**E**). The area between the vertical dotted line (2D) is the healing tissue that have not yet completed remodeling. The asterisk indicates inflammatory cell infiltration, the black arrow indicates small vessels. (**F** and **G**) Images of CD31 staining in the wounded skin at D15 and quantification of $CD31^+$ vessel area (% total area). Scale bar, 500 μm (low magnification) and 100 μm (high magnification). (**H** and **I**) Images of vWF staining in the wounded skin at D15 and quantification of vWF^+ vessel area (% total area). Scale bar, 500 μm (low magnification) and 100 μm (high magnification). (**J**) CD31 and 4HNE co-staining of the wounded skin. The asterisk indicates the co-location region. Scale bar, 50 μm. $^{**}p < 0.01$ by student's *t* test.

Abbreviations: Ep, epidermis; HF, hair follicle; AT, adipose tissue; ns, no significance.

https://doi.org/10.2147/IJN.S527475

exhibited a reduction in hair follicle density and increased subcutaneous adipose tissue thickness. To deeply analyze the characteristics of skin structure and vascularization, immunofluorescence staining for CD31 and von Willebrand factor (vWF) was performed on selected magnified skin areas (Figure 2B). It can be observed that the epidermal layer, which was originally thin with only 1–2 layers of epithelial cells, has become thicker with 3–5 layers of epithelial cells in HFD mice. Although dermal thickness (papillary and reticular layers) remained largely unchanged, a significant increase in dermal gland density was observed in the HFD group. Quantitative analysis of CD31 and vWF staining demonstrated no significant difference in the vascularization level of the normal skin between groups (Figure 2C).

Next, the skin wound healing process after injury in HFD mice was explored. Histological analysis of the wounded skin at D15 post-wounding revealed significantly larger central scar areas in HFD mice compared to Ctrl mice (Figure 2D). Extensive scabbing persisted on the wound surface of HFD mice. Furthermore, the central wound region in HFD mice exhibited persistent infiltration of inflammatory cells and necrotic debris, in contrast to the re-epithelialization observed in Ctrl group (Figure 2E). Hair follicle regeneration was evident at the wound periphery in Ctrl mice, while HFD wounds displayed a prominent layer of subcutaneous adipose tissue. H&E staining revealed abundant mature microvessels with luminal endothelium in both the wound center and edge areas of Ctrl mice, while HFD wounds displayed immature microvasculature. Moreover, CD31 and vWF staining of wounded skin at D15 directly confirmed declined vascularization level in HFD mice (Figure 2F–I). The hyperglycemic and hyperlipidemic environment, coupled with the accumulation of toxic metabolites in diabetes, highly likely contributed to tissue damage, particularly affecting vascular endothelial cells that are in direct contact with blood. Ferroptosis is driven by iron-dependent lipid peroxidation due to the impaired antioxidant defense system. Co-staining of vascular endothelial cells (CD31) and the lipid peroxidation product 4-hydroxynonenal (4HNE) demonstrated significant 4HNE accumulation within the $CD31^{+}$ vessels, suggesting that ferroptosis occurred in vascular endothelial cells during the diabetic skin healing process (Figure 2J).

Based on previous researches, extracellular vesicles (EVs) are cell-derived acellular entities that mediate information exchange in the circulation, carrying a wealth of bioactive molecules. To further verify the impact of diabetes on endothelial cell function, circulating EVs were isolated from both kinds of mice and co-cultured with endothelial cells in vitro to mimic the microenvironment of vascular endothelial cells in vivo (Figure 3A). Both circulating EVs from Ctrl-mice (CEVs) and HFD-mice (HEVs) displayed typical cup-shaped vesicles with a diameter of approximately 100 nm under transmission electron microscopy (TEM) (Figure 3B). Nano flow cytometry (NanoFCM) analysis demonstrated a particle distribution range of CEVs and HEVs from 50 to 200 nm (Figure 3C). Western blotting further confirmed the expression of EV markers (CD63, Alix, TSG101) and absence of the negative marker (Calnexin), verifying the purity of the isolated EVs (Figure 3D). Fluorescence microscopy demonstrated significant EVs uptake by ECs, no significance observed between HEVs and CEVs (Figure 3E), thus simulating the real response of vascular endothelial cells in contact with circulation in vivo. After 48 hours of co-incubation, HEVs led to a significant decrease in endothelial cell viability (Figure 3F). An in-depth exploration revealed that HEVs exposure led to a significant increase in intracellular reactive oxygen species (ROS) production (Figure 3G). Consistently, HEVs also increased mitochondrial ROS (mtROS) level, as detected using the mitoSOX probe (Figure 3G). These findings suggested that HEVs induced oxidative stress damage in ECs. To determine whether diabetes induced ferroptosis in endothelial cells, ferrostatin-1 (Fer-1), a known ferroptosis inhibitor, was used as a negative control. Fer-1 effectively attenuated the HEVs-induced reduction in cell viability and ROS generation in the cytoplasm and mitochondria (Figure 3F and G). Additionally, C11-BODIPY staining demonstrated increased lipid peroxidation level in HEVs-treated ECs, which was reversed by Fer-1 (Figure 3H). These data strongly suggested that diabetes induced EC ferroptosis.

Next, the functional consequences of HEVs exposure on ECs were further evaluated in vitro. HEVs obviously reduced the proliferation rate of ECs, as determined by Ki-67 immunostaining (Figure 3I). The cell scratch assay demonstrated that HEVs decreased the migration rate of ECs at different timepoints, which is an important property of ECs during angiogenesis (Figure 3J and K). In the tube formation assay, HEVs-treated ECs formed fewer, shorter, and less-organized tube structures compared to CEVs group (Figure 3L). The application of Fer-1 strikingly rescued the impairment of proliferation, migration, and tube-forming ability of ECs caused by HEVs (Figure 3I–L). Altogether, these results strongly indicate that diabetes impairs angiogenesis by inducing ferroptosis of endothelial cells.

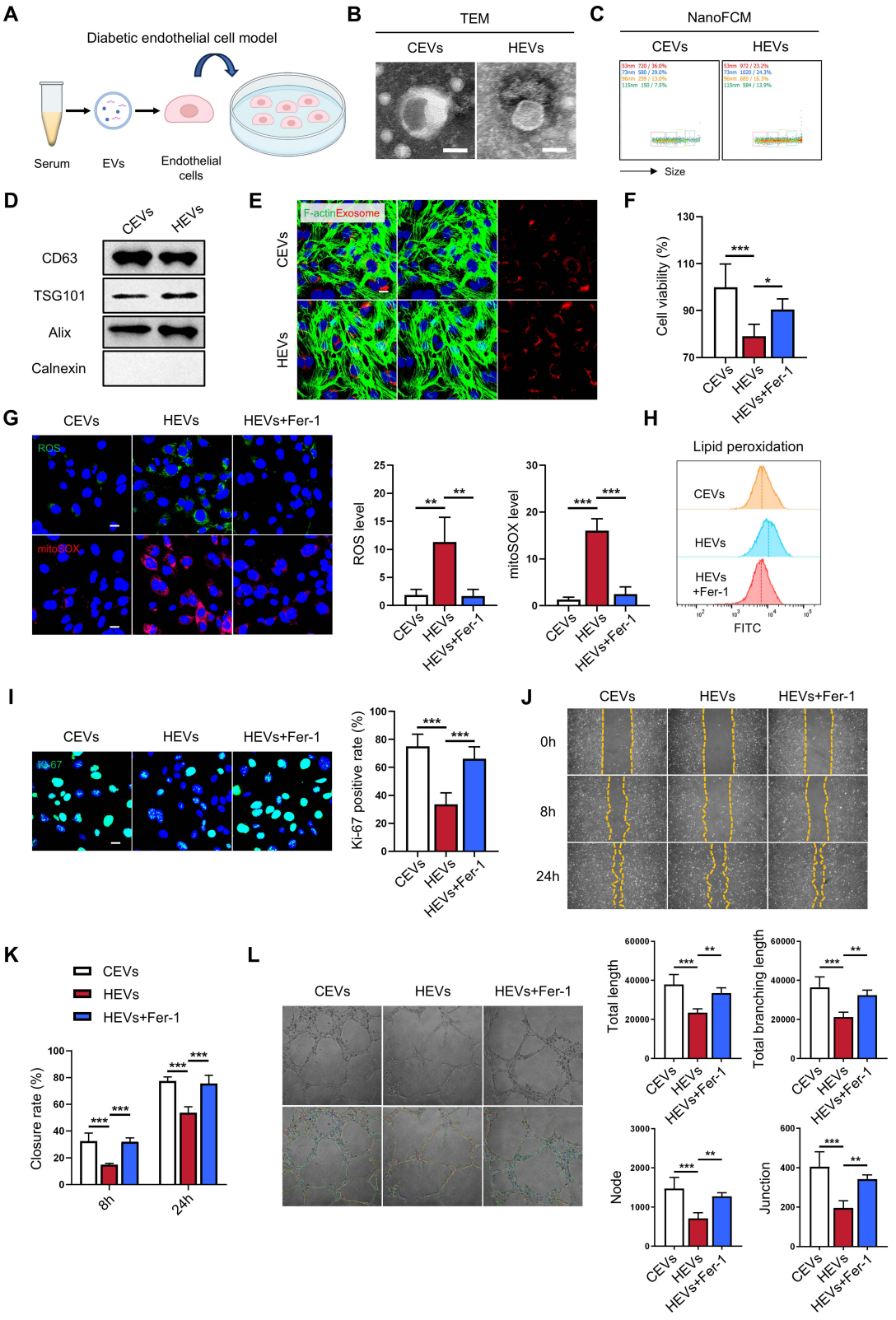

Figure 3 Diabetes induced ferroptosis of endothelial cells in vitro. (**A**) Establishment of diabetic endothelial cell model in vitro. (**B**) Transmission Electron Microscopy (TEM) images of Ctrl mice-derived EVs (CEVs) and HFD mice-derived EVs (HEVs). Scale bar, 50 nm. (**C**) Nano flow cytometry analysis of CEVs and HEVs. (**D**) Western blotting analysis of surface markers in CEVs and HEVs. (**E**) Fluorescence images of the internalization of CEVs and HEVs by endothelial cells. Scale bar, 20 μm. (**F**) Cell viability of endothelial cells after EVs treatment. (**G**) Images and quantification of cellular ROS level and mitochondrial ROS level in endothelial cells after EVs treatment. Scale bar, 20 μm. (**H**) Lipid peroxidation level in endothelial cells assessed by flow cytometry using C11-BODIPY. (**I**) Images and quantification of Ki-67 level in endothelial cells. Scale bar, 20 μm. (**J**) Cell migration ability of endothelial cells by cell scratch assay. (**K**) Quantification of scratch closure rate. (**L**) Images and quantitative analysis of tube formation assay in endothelial cells. *$p < 0.05$, **$p < 0.01$ and ***$p < 0.001$ by one-way ANOVA.

https://doi.org/10.2147/IJN.S527475

Isolation and Characterization of Adipose Stem Cell-Derived Apoptotic Vesicles

Adipose tissue was excised from the inguinal region of mice, and adipose tissue-derived stem cells were isolated and cultured (Figure 4A). Flow cytometry analysis showed that the extracted cells expressed the positive markers of mesenchymal stem cells (CD73, CD90 and CD105), while not expressing the hematopoietic lineage markers (CD45, CD11b) (Figure 4B). Light microscopy revealed a typical fibroblast-like morphology with a long spindle shape across multiple passages (Figure 4C, I–III). Moreover, they had the ability to form single-cell clones (Figure 4C, IV). After osteogenic induction, alizarin red staining revealed the formation of mineralized nodules, indicative of osteogenic differentiation (Figure 4C, V). Similarly, adipogenic differentiation ability was also confirmed by Oil Red O staining (Figure 4C, VI). All these results demonstrated the mesenchymal stem cell (MSC) characteristics of the isolated cells, thus identifying them as adipose stem cells (ASCs).

To obtain apoptotic vesicles (apoVs), apoptosis of ASCs was induced in vitro using staurosporine (sts), followed by differential centrifugation (Figure 4D). After treatment with sts for 4 h, ASCs displayed a characteristic withered branch-

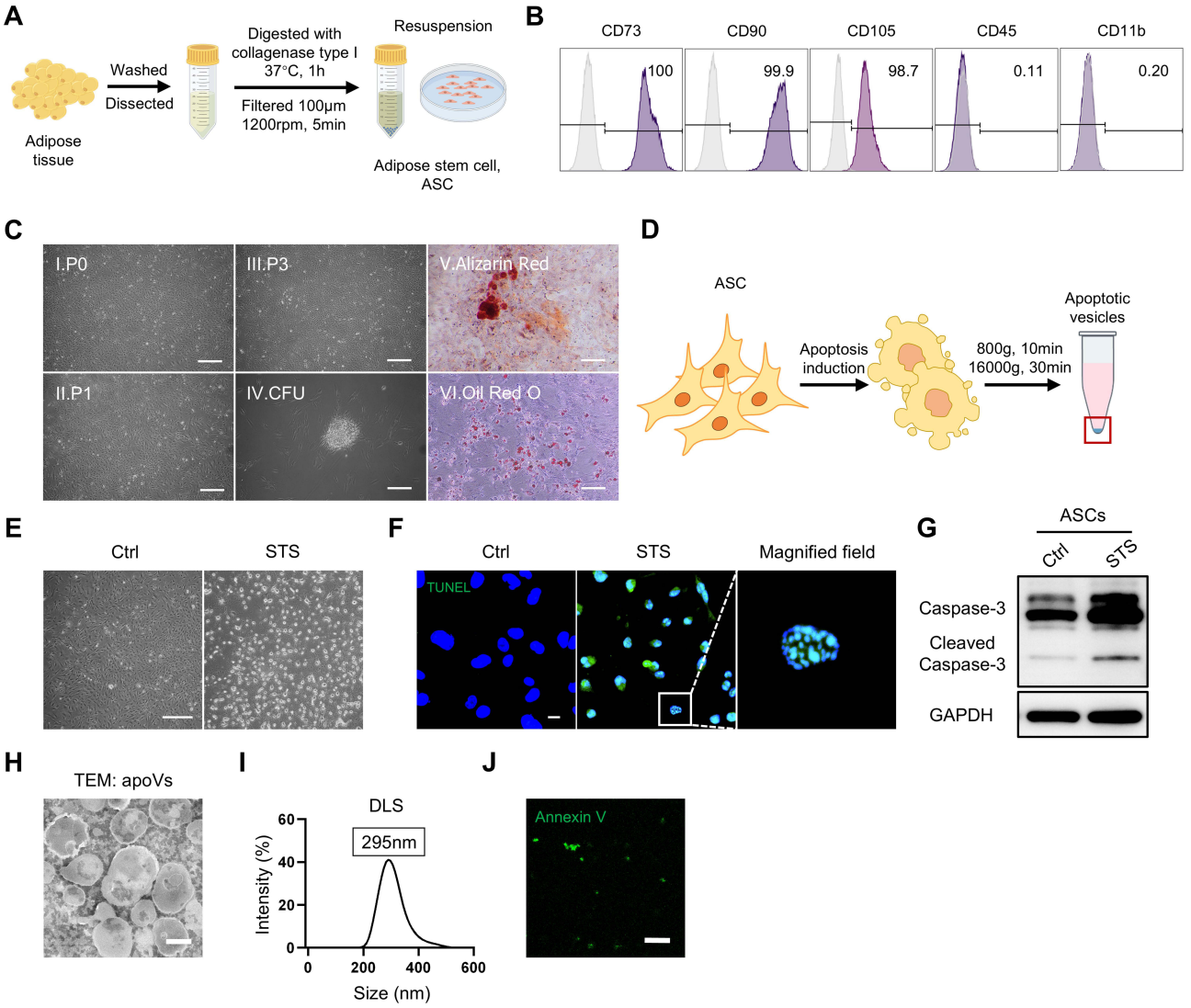

Figure 4 Isolation and characterization of adipose stem cells and apoptotic vesicles. (**A**) The schematic illustration of the isolation process for adipose stem cells (ASCs). (**B**) The expression of ASCs surface markers was detected by flow cytometry. Positive markers: CD73, CD90, CD105. Negative markers: CD45, CD11b. (**C**) Morphology, clone forming unit, osteogenic and adipogenic differentiation images of ASCs. Scale bar, 500 μm (I–III), 200 μm (IV–VI). (**D**) Isolation of apoptotic vesicles (apoVs) from ASCs. (**E**) Images of Ctrl and staurosporine (sts)-treated ASCs. Scale bar, 500 μm. (**F**) TUNEL staining of Ctrl and sts-treated ASCs. Scale bar, 20 μm. (**G**) Western blotting analysis of Ctrl and sts-treated ASCs. (**H**) Transmission electron microscope (TEM) images of apoVs. Scale bar, 200 nm. (**I**) Size distribution of apoVs by dynamic light scattering analysis. (**J**) Annexin V staining of apoVs. Scale bar, 10 μm.

like morphology under light microscopy (Figure 4E). TUNEL assay confirmed 100% apoptotic rate in sts-treated ASCs. These sts-treated ASCs exhibited typical apoptotic morphology, characterized by nuclear condensation and fragmentation (Figure 4F). Western blotting analysis detected the cleaved caspase-3 in apoptotic ASCs, confirming the occurrence of apoptosis (Figure 4G). TEM showed that the isolated apoVs exhibited spherical bodies with an approximate diameter of 200–300 nm (Figure 4H). Dynamic light scattering (DLS) analysis yielded a particle size distribution curve with a peak at approximately 295 nm (Figure 4I). Annexin V staining demonstrated phosphatidylserine externalization on the apoptotic membrane surface (Figure 4J). These results demonstrated the successful isolation and characterization of ASCs and their secreted apoVs, preparing for further cell experiments and diabetic wound treatment.

ASC-apoVs Inhibited Ferroptosis to Reverse Dysfunction of Endothelial Cells

To verify the therapeutic potential of ASCs-apoVs on regulating endothelial cells function impaired by diabetes, apoVs were firstly applied to endothelial cells exposed to HEVs to assess their effect on ECs ferroptosis. Cell viability assay demonstrated the beneficial fact that apoVs notably mitigated the ferroptosis level of ECs induced by HEVs (Figure 5A).

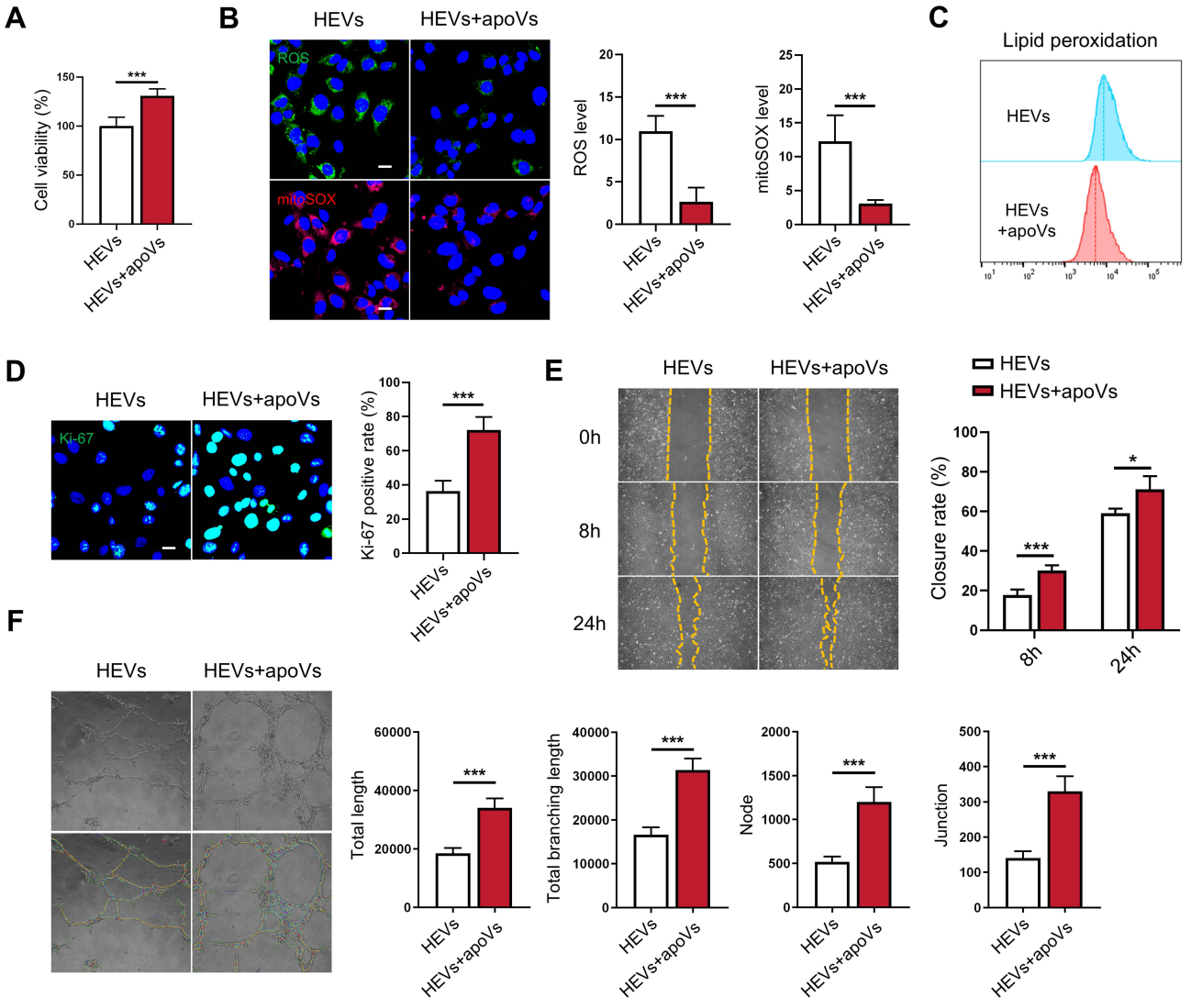

Figure 5 ASCs-apoVs rescued ferroptosis of endothelial cells in vitro. (**A**) Cell viability of diabetic endothelial cells treated with apoVs. (**B**) Images and quantification of cellular ROS level and mitochondrial ROS level in diabetic endothelial cells treated with apoVs. Scale bar, 20 μm. (**C**) Lipid peroxidation level in diabetic endothelial cells treated with apoVs detected using C11-BODIPY. (**D**) Images and quantification of Ki-67 level in diabetic endothelial cells treated with apoVs. Scale bar, 20 μm. (**E**) Cell scratch assay and scratch closure rate of diabetic endothelial cells treated with apoVs. (**F**) Images and quantitative analysis of tube formation assay in diabetic endothelial cells treated with apoVs. *$p < 0.05$, ***$p < 0.001$ by student's *t* test.

https://doi.org/10.2147/IJN.S527475

The accumulation of cytosolic and mitochondrial ROS in ECs caused by HEVs was greatly alleviated by the application of apoVs (Figure 5B), promoting cell survival and function. Meanwhile, ASC-apoVs significantly reduced HEVs-induced lipid peroxidation in ECs (Figure 5C). These results indicate the protective effect of ASC-apoVs against HEVs-induced ferroptosis in ECs.

Based on this, the effect of apoVs on angiogenic-related function of ECs was further investigated. It was noticeable that apoVs increased the proliferation rate of HEVs-treated ECs from 36.38% to 72.12% evidenced by Ki-67 immunostaining (Figure 5D). Additionally, ASC-apoVs significantly enhanced the migration capacity of HEVs-treated ECs, as demonstrated by increased wound closure rates in a scratch assay by 12.45% at 8 h, and 11.94% 24 h (Figure 5E), respectively. The tube formation assay directly demonstrated that apoVs significantly promoted the tube forming capacity of HEVs-treated ECs (Figure 5F). Quantitative analysis revealed significant improvements in total length, total branching length and overall network complexity. These evidence prove that ASC-apoVs effectively mitigate ferroptosis in diabetic endothelial cells, thereby reversing the impairment of their functions under the pathological state of diabetes, establishing a rationale for in vivo application.

Application of ASC-apoVs Improved Vascularization and Accelerated Wound Healing

Following in vitro confirmation of ASC-apoVs efficacy in mitigating EC ferroptosis, their therapeutic efficacy in diabetic wound healing was investigated in vivo. Skin wounds were prepared on HFD-induced diabetic mouse model with topical treatment of apoVs on the wound at D0, D3, D6 and D9 post-wounding, with wound healing assessed until D15 (Figure 6A). The impact of ASC-apoVs on wound vascularization and EC function was initially assessed. Immunofluorescence staining showed that apoVs significantly reduced the enrichment level of 4HNE within the wound vasculature (Figure 6B), suggesting that apoVs effectively inhibit ferroptosis of endothelial cells in vivo. Furthermore, apoVs also remarkably increased the density of newly formed ($CD31^+$) and mature (vWF^+) blood vessels in both the center and edge areas of the wounded skin in HFD mice (Figure 6C–F), which would be conducive to diabetic wound healing and remodeling.

Given the observed improvement in vascularization, the effects of ASC-apoVs on overall wound healing were further investigated. Quantitative analysis of wound closure rates showed that apoVs significantly accelerated wound healing in HFD mice by 13.13% at D5 (p^*=0.036), 25.29% at D10 (p^{***}<0.001), 3.77% at D15 (p^{***}<0.001) (Figure 7A and B).

Histological analysis provided further evidence for the enhanced healing observed in the ASC-apoVs group. At D15, there still remained obvious scab on the wound surface in HFD mice because the unclosed wound requires a replacement tissue to prevent secondary damage, but apoVs promoted wound closure and epithelial barrier formation (Figure 7C). ASC-apoVs treatment was associated with reduced subcutaneous adipose tissue and increased hair follicle density in HFD mice (Figure 7C). Detailed histological analysis of HFD wounds revealed substantial inflammatory cell infiltration in the transitional healing tissue in the center wound region (Figure 7D). While partial re-epithelialization was observed at the wound edge region in HFD mice, the epithelial layer was significantly more organized and mature in the apoVs-treated group. Intact microvascular structures were evident throughout apoVs-treated wounds, in contrast to the numerous vessel-like structures lacking mature endothelium in wounds of HFD mice. In addition, the functional recovery of the healed skin was assessed using specific markers. Epithelial barrier formation is critical for maintaining skin integrity. Immunostaining for cytokeratin 14 (CK14) revealed significantly increased CK14 expression in the epithelium of apoVs-treated wounds compared to HFD wounds (Figure 7E and F). Collagen deposition in the subcutaneous tissue is crucial for maintaining skin biomechanical properties. Immunofluorescence staining revealed significantly increased collagen III (COL3) expression and a more organized collagen fiber distribution in the skin after apoVs treatment, which is the basic condition for skin elasticity and toughness (Figure 7G and H). Collectively, this study demonstrates that adipose stem cell-derived apoptotic vesicles (ASC-apoVs) effectively mitigate lipid peroxidation and ferroptosis of endothelial cells, thereby promoting angiogenesis and accelerating diabetic wound healing, highlighting their significant therapeutic potential in functional wound repair (Figure 8).

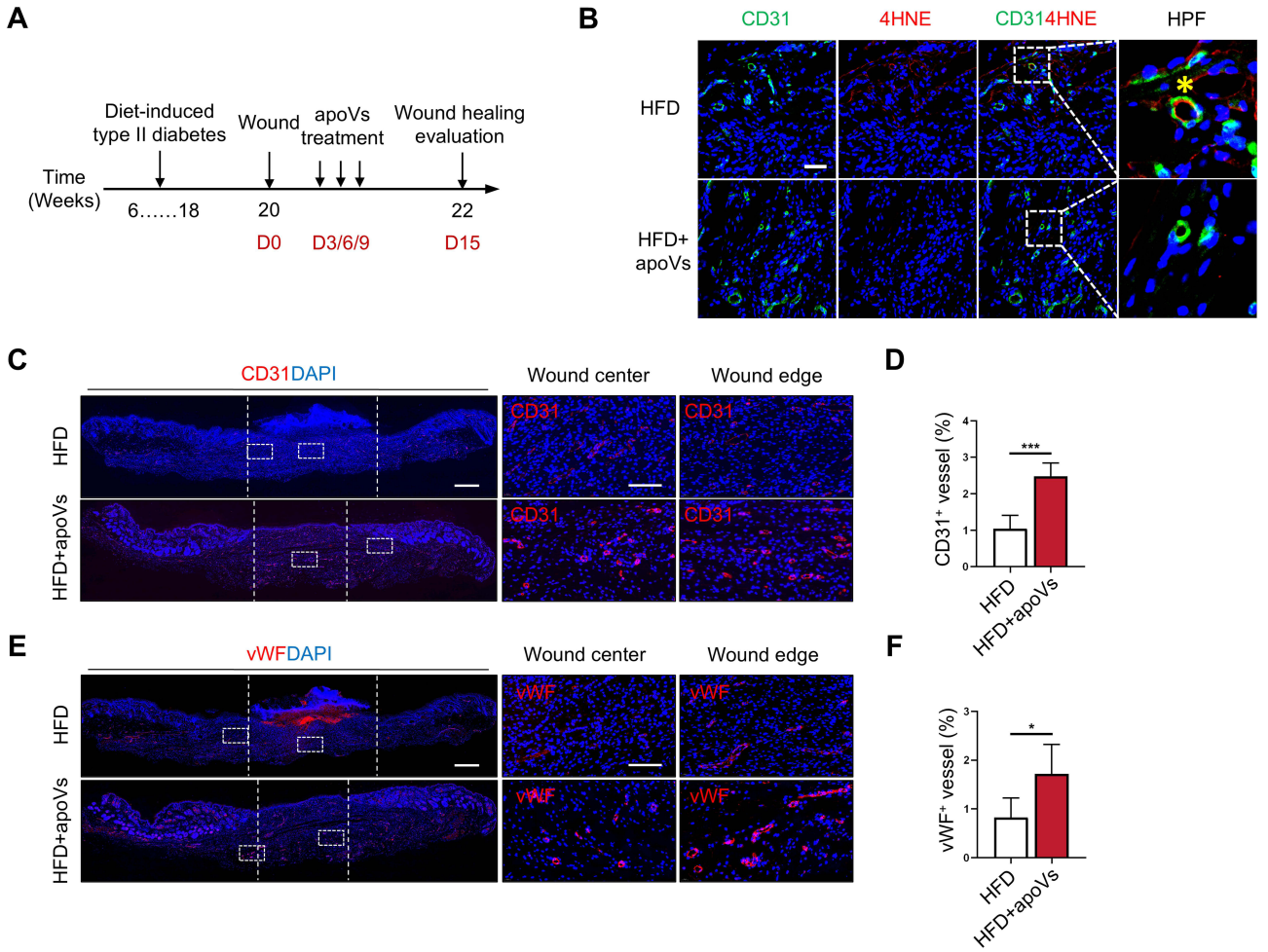

Figure 6 ASCs-apoVs inhibited ferroptosis of endothelial cells and promoted vascularization of diabetic wound in vivo. (**A**) The schematic illustration of apoVs treatment regimen in diabetic wound model. (**B**) CD31 and 4HNE co-staining of the wounded skin. The asterisk indicates the co-location region. Scale bar, 50 μm. (**C** and **D**) Images of CD31 staining in the wounded skin at D15 and quantification of $CD31^+$ vessel area (% total area). Scale bar, 500 μm (low magnification) and 100 μm (high magnification). (**E** and **F**) Images of vWF staining in the wounded skin at D15 and quantification of vWF^+ vessel area (% total area). Scale bar, 500 μm (low magnification) and 100 μm (high magnification). *$p < 0.05$, ***$p < 0.001$ by student's *t* test.

Discussion

Diabetes, a global chronic disease, significantly impairs wound healing, thereby detrimentally affecting patients' health and quality of life. Although angiogenesis disorder has been identified as a critical obstacle hindering diabetic wound healing, the lack of a core pathogenic mechanism has led to blindness in treatment strategies. Traditional studies have primarily concentrated on the vascular damage induced by hyperglycemia and oxidative stress in the diabetes.[23,42] In contrast, our previous findings indicated that, from the perspective of metabolic homeostasis and interorgan crosstalk, the secondary damage induced by diabetes largely results from compensatory metabolic alterations following the disruption of the primary metabolic mechanisms.[43] This study explored the role of ferroptosis in the angiogenesis disorders in the context of dysregulated lipid metabolism, enriching the theoretical framework of the pathophysiological mechanisms underlying diabetic wound healing. Ferroptosis is closely related to cellular oxidative stress damage, and has been widely concerned in the pathological process of many diseases in recent years.[44,45] Based on the pathological features of diabetes, we hypothesized that oxidative stress and dyslipidemia render endothelial cells more susceptible to ferroptosis, thus impairing angiogenesis and hindering wound healing. Our findings underscore the importance of considering both glucose control and the impact of lipid metabolic dysfunction in the treatment of diabetic wounds.

In the diabetic environment, metabolic disturbances and compromised antioxidant defenses led to the lipid peroxidation reaction in endothelial cells, ultimately triggering ferroptosis. This discovery not only deepens the understanding of

https://doi.org/10.2147/IJN.S527475

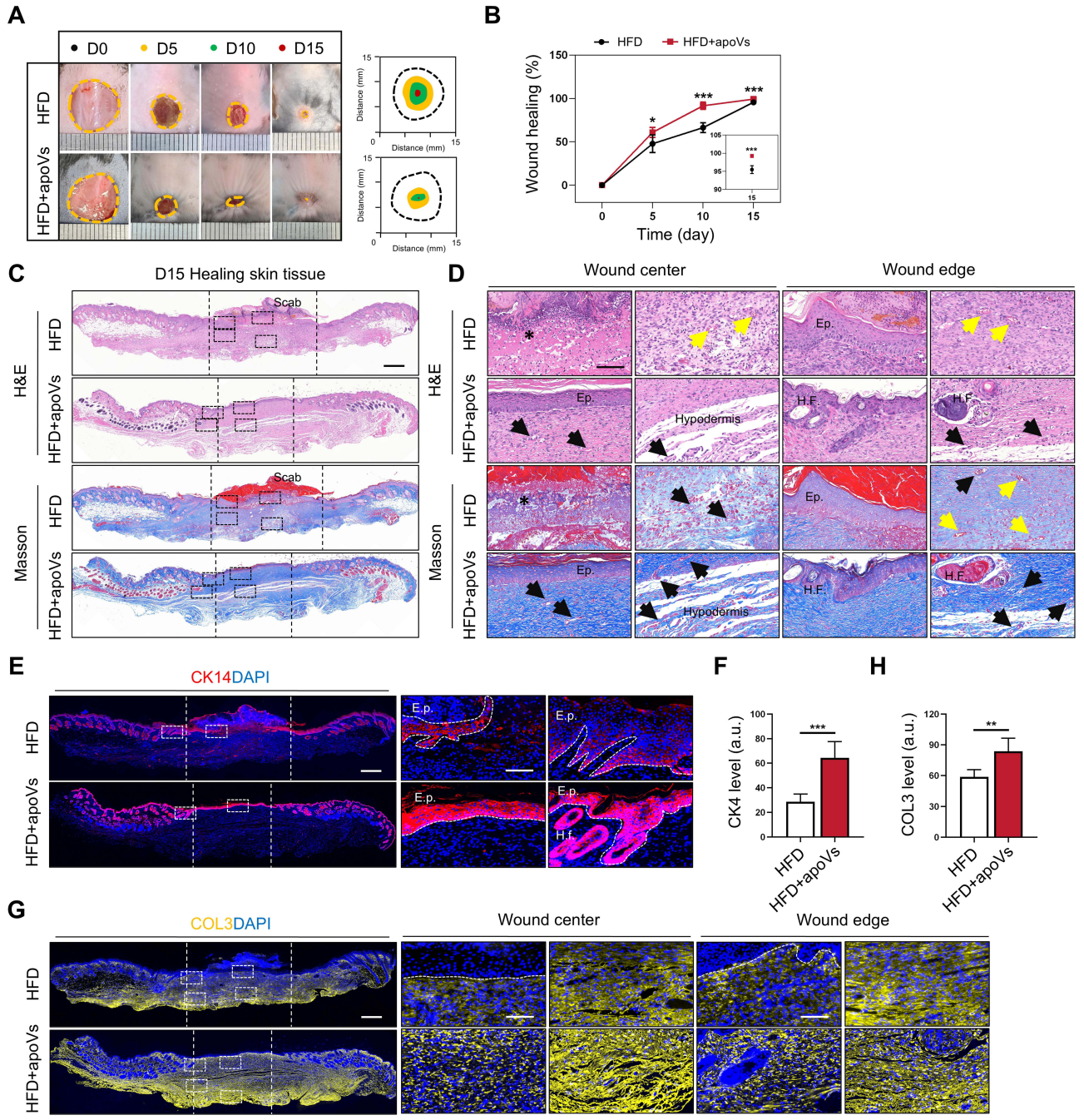

Figure 7 ASCs-apoVs accelerated diabetic wound healing and functional regeneration. (**A** and **B**) Representative photographs of cutaneous wounds and quantitative analysis of the wound healing rate in each group. (**C** and **D**) H&E and Masson staining of the wounded skin from HFD mice and HFD+apoVs mice at D15. The high-magnified images of the dotted box area in the center and edge of the wound (**C**) are shown in (**D**). Scale bar, 500 μm (**C**) and 100 μm (**D**). The area between the vertical dotted line (**C**) is the healing tissue that have not yet completed remodeling. Ep., epidermis; H.F., hair follicle. The asterisk indicates inflammatory cell infiltration, the black arrow indicates small vessels, the yellow arrow indicates immature vessel-like structure. (**E** and **F**) Images of CK14 staining in the wounded skin at D15 and quantification of CK14 level. Scale bar, 500 μm (low magnification) and 100 μm (high magnification). (**G** and **H**) Images of COL3 staining in the wounded skin at D15 and quantification of COL3 level. Scale bar, 500 μm (low magnification) and 100 μm (high magnification). *$p < 0.05$, **$p < 0.01$ and ***$p < 0.001$ by student's t test.

the pathological mechanism of poor diabetic wound healing, but also provides a specific target for subsequent interventions. Apoptotic products, a set of substances highly conserved in biological evolution, have been implicated in modulating inflammatory responses and cellular fate decisions.[34–37,46] In the context of diabetic wound healing, the occurrence of ferroptosis in endothelial cells due to the diabetic environment, highlights the need to explore the potential therapeutic effects of apoptotic products. Notably, we successfully isolated secretory apoptotic vesicles from adipose

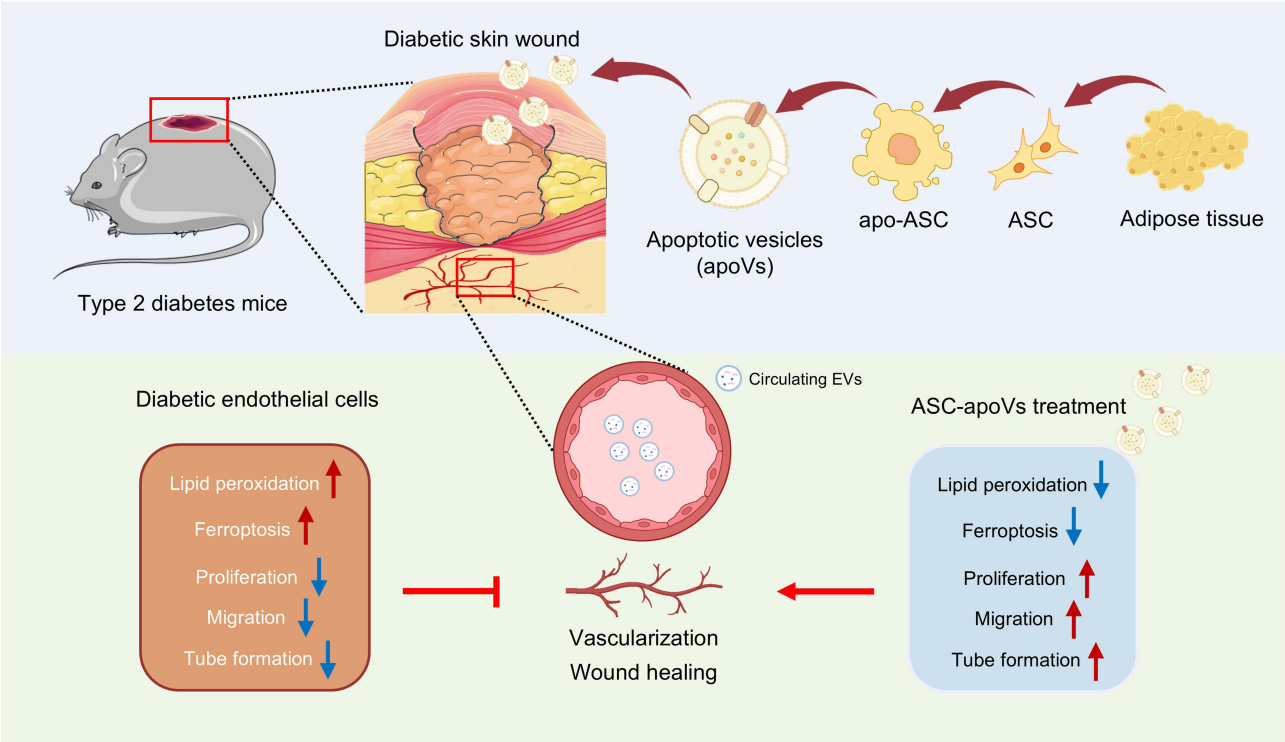

Figure 8 Schematic illustration of the mechanism by which ASC-apoVs promote diabetic wound healing.

stem cells and demonstrated their positive role in promoting diabetic wound healing. In both in vitro and in vivo experiments, ASC-apoVs effectively inhibited ferroptosis in endothelial cells, while simultaneously enhancing their proliferation, migration and angiogenic activities of endothelial cells, thereby promoting wound healing. Compared with cell therapy, ASCs-apoVs, as a cell-free therapeutic approach, avoid the challenges associated with cell quality control and cell heterogeneity. Consequently, ASC-apoVs present a safer and more stable treatment alternative with significant clinical translational potential. Damaged cells often initiate autophagy to clear damaged organelles and misfolded proteins, thereby facilitating repair and reestablishing cellular homeostasis.[47] Recent studies have demonstrated that apoVs significantly enhance autophagic activity in endothelial cells to promote vascularization during dental pulp regeneration and post-myocardial infarction tissue repair.[32,48] The autophagy-regulating capacity of apoVs raises the hypothesis that they may participate in regulating lipid metabolism and oxidative stress via autophagic pathways to counteract ferroptosis in diabetic wounds, thereby promoting wound healing, which warrants further investigation.

Compared with previous studies, this study offers some unique innovations to the field. While most existing research on diabetic wound treatment has focused on growth factors and extracellular matrix components,[16,49] there has been limited exploration of the therapeutic potential of apoptotic derivatives derived from stem cells. At the same time, existing studies pay little attention to the relationship between ferroptosis, an emerging cell death mode, and angiogenesis in diabetic wound healing.[19,42,50] Our findings clarify the critical role of endothelial cell ferroptosis in impaired angiogenesis in diabetic wounds, and elucidate the mechanism through which ASCs-apoVs promotes angiogenesis by inhibiting ferroptosis. These insights provide an important theoretical foundation for subsequent investigations. However, there are still limitations in this study. Firstly, the effector molecules, molecular pathways, and regulatory targets involved in the inhibition of endothelial cell ferroptosis by ASC-apoVs warrant further investigation. Secondly, although our findings are promising, future clinical trials are required to validate the safety and efficacy of ASC-apoVs in human patients. While cell-free therapies like apoVs offer advantages in stability and biocompatibility, their translational potential still requires cost-effectiveness evaluations. This includes optimizing production scalability, storage protocols, and delivery systems to align with clinical affordability standards. Large-scale production of high-purity and bioactive

ASC-apoVs, maintaining their stability during storage and transport, and ensuring their efficient delivery to the wound site are critical challenges that must be addressed.

In conclusion, this study revealed that endothelial cell ferroptosis is one of the main mechanisms of diabetic vascular damage. ASC-apoVs, as a potential cell-free therapy, open a new avenue for the treatment of diabetic wounds. In the future, in-depth research on the molecular mechanism and preparation process is expected to promote the further development of the field of diabetes wound treatment and bring better prospects for diabetic patients.

Conclusion

In conclusion, this study identifies endothelial cell ferroptosis as a key mechanism contributing to vascular damage and impaired wound healing in diabetes. Adipose stem cell-derived apoptotic vesicles (ASC-apoVs) represent a promising cell-free therapeutic strategy for treating diabetic wounds. When administered at a dose of 200 μg (protein content) via subcutaneous injection around the wound site on days 3, 6, and 9 post-injury, ASC-apoVs mitigate lipid peroxidation-induced endothelial cell ferroptosis, and promote angiogenesis to accelerate wound healing. This dosing regimen significantly improved vascular density and reepithelialization rates in diabetic wound models, providing proof-of-concept for ASC-apoVs as a viable therapeutic approach. This study provides new insights into the metabolism-related mechanisms underlying endothelial cell damage in diabetes and offers a novel therapeutic avenue for the development of targeted, cell-free therapies for diabetic wound treatment.

Abbreviations

HFD, high-fat diet; ASC, adipose stem cell; apoVs, apoptotic vesicles; AUC, area under curve; IPGTT, intraperitoneal glucose tolerance test.

Author Contributions

All authors made a significant contribution to the work reported, whether that is in the conception, study design, execution, acquisition of data, analysis and interpretation, or in all these areas; took part in drafting, revising or critically reviewing the article; gave final approval of the version to be published; have agreed on the journal to which the article has been submitted; and agree to be accountable for all aspects of the work.

Funding

This study was supported by National Natural Science Foundation of China (82301027 to G.D.), China Postdoctoral Science Foundation (2023M734280 to G.D.), National Natural Science Foundation of China (82170925 to S.L.), National Postdoctoral Program for Innovative Talents of China (BX20220394 to G.D.).

Disclosure

The authors report no conflicts of interest in this work.

References

1. Jiao Q, Zhi L, You B, Wang G, Wu N, Jia Y. Skin homeostasis: mechanism and influencing factors. *J Cosmetic Dermatol*. 2024;23:1518–1526. doi:10.1111/jocd.16155
2. Gribonika I, Band VI, Chi L, et al. Skin autonomous antibody production regulates host-microbiota interactions. *Nature*. 2025;638:1043–1053. doi:10.1038/s41586-024-08376-y
3. Tsokos GC. Autoimmunity and organ damage in systemic lupus erythematosus. *Nat Immunol*. 2020;21:605–614. doi:10.1038/s41590-020-0677-6
4. Druskovich C, Kelley J, Aubrey J, Palladino L, Wright GP. A review of melanoma subtypes: genetic and treatment considerations. *J Surg Oncol*. 2024;131:356–364. doi:10.1002/jso.27953
5. Polk C, Sampson MM, Roshdy D, Davidson LE. Skin and soft tissue infections in patients with diabetes mellitus. *Infect Dis Clin North Am*. 2021;35:183–197. doi:10.1016/j.idc.2020.10.007
6. Khan AW, Jandeleit-Dahm KAM. Atherosclerosis in diabetes mellitus: novel mechanisms and mechanism-based therapeutic approaches. *Nat Rev Cardiol*. 2025;22:482–496. doi:10.1038/s41569-024-01115-w
7. Veith AP, Henderson K, Spencer A, Sligar AD, Baker AB. Therapeutic strategies for enhancing angiogenesis in wound healing. *Adv Drug Deliv Rev*. 2019;146:97–125. doi:10.1016/j.addr.2018.09.010

8. Peña OA, Martin P. Cellular and molecular mechanisms of skin wound healing. *Nat Rev Mol Cell Biol*. 2024;25:599–616. doi:10.1038/s41580-024-00715-1
9. Rahimi F, Ahmadkhani N, Goodarzi A, et al. Gelatin-based hydrogel functionalized with taurine moieties for in vivo skin tissue regeneration. *Biodes Manuf*. 2023;6:284–297. doi:10.1007/s42242-022-00227-x
10. Synofzik J, Heene S, Jonczyk R, Blume C. Ink-structing the future of vascular tissue engineering: a review of the physiological bioink design. *Biodes Manuf*. 2024;7:181–205. doi:10.1007/s42242-024-00270-w
11. Liu J, Zhang Y, Liu C, et al. A single dose of VEGF-A circular RNA sustains in situ long-term expression of protein to accelerate diabetic wound healing. *J Control Release*. 2024;373:319–335. doi:10.1016/j.jconrel.2024.07.018
12. Li P, Ruan L, Jiang G, et al. Design of 3D polycaprolactone/ε-polylysine-modified chitosan fibrous scaffolds with incorporation of bioactive factors for accelerating wound healing. *Acta Biomater*. 2022;152:197–209. doi:10.1016/j.actbio.2022.08.075
13. Cole JB, Florez JC. Genetics of diabetes mellitus and diabetes complications. *Nat Rev Nephrol*. 2020;16:377–390. doi:10.1038/s41581-020-0278-5
14. Longo VD, Mattson MP. Fasting: molecular mechanisms and clinical applications. *Cell Metab*. 2014;19:181–192. doi:10.1016/j.cmet.2013.12.008
15. Saltiel AR, Olefsky JM. Inflammatory mechanisms linking obesity and metabolic disease. *J Clin Invest*. 2017;127:1–4. doi:10.1172/JCI92035
16. Yang J, Chen Z, Pan D, Li H, Shen J. Umbilical cord-derived mesenchymal stem cell-derived exosomes combined pluronic F127 hydrogel promote chronic diabetic wound healing and complete skin regeneration. *Int J Nanomed*. 2020;15:5911–5926. doi:10.2147/IJN.S249129
17. Iannotta D, A A, Kijas AW, Rowan AE, Wolfram J. Entry and exit of extracellular vesicles to and from the blood circulation. *Nat Nanotechnol*. 2024;19:13–20. doi:10.1038/s41565-023-01522-z
18. Zheng D, Liu J, Piao H, Zhu Z, Wei R, Liu K. ROS-triggered endothelial cell death mechanisms: focus on pyroptosis, parthanatos, and ferroptosis. *Front Immunol*. 2022;13:1039241. doi:10.3389/fimmu.2022.1039241
19. Liu P, Zhang Z, Cai Y, Li Z, Zhou Q, Chen Q. Ferroptosis: mechanisms and role in diabetes mellitus and its complications. *Ageing Res Rev*. 2024;94:102201. doi:10.1016/j.arr.2024.102201
20. Miao R, Fang X, Zhang Y, Wei J, Zhang Y, Tian J. Iron metabolism and ferroptosis in type 2 diabetes mellitus and complications: mechanisms and therapeutic opportunities. *Cell Death Dis*. 2023;14:186. doi:10.1038/s41419-023-05708-0
21. Wang Z, Wu C, Yin D, Dou K. Ferroptosis: mechanism and role in diabetes-related cardiovascular diseases. *Cardiovasc Diabetol*. 2025;24:60. doi:10.1186/s12933-025-02614-x
22. Strain WD, Paldánius PM. Diabetes, cardiovascular disease and the microcirculation. *Cardiovasc Diabetol*. 2018;17:57. doi:10.1186/s12933-018-0703-2
23. Giacco F, Brownlee M. Oxidative stress and diabetic complications. *Circ Res*. 2010;107:1058–1070. doi:10.1161/CIRCRESAHA.110.223545
24. Zakrzewski W, Dobrzyński M, Szymonowicz M, Rybak Z. Stem cells: past, present, and future. *Stem Cell Res Ther*. 2019;10:68. doi:10.1186/s13287-019-1165-5
25. Hoang DM, Pham PT, Bach TQ, et al. Stem cell-based therapy for human diseases. *Signal Transduct Target Ther*. 2022;7:272. doi:10.1038/s41392-022-01134-4
26. Margiana R, Markov A, Zekiy AO, et al. Clinical application of mesenchymal stem cell in regenerative medicine: a narrative review. *Stem Cell Res Ther*. 2022;13:366. doi:10.1186/s13287-022-03054-0
27. Krampera M, Le Blanc K. Mesenchymal stromal cells: putative microenvironmental modulators become cell therapy. *Cell Stem Cell*. 2021;28:1708–1725. doi:10.1016/j.stem.2021.09.006
28. Zhou T, Yuan Z, Weng J, et al. Challenges and advances in clinical applications of mesenchymal stromal cells. *J Hematol Oncol*. 2021;14:24. doi:10.1186/s13045-021-01037-x
29. Levy O, Kuai R, Siren EMJ, et al. Shattering barriers toward clinically meaningful MSC therapies. *Sci Adv*. 2020;6:eaba6884. doi:10.1126/sciadv.aba6884
30. Fu Y, He Y, Wu D, et al. Apoptotic vesicles: emerging concepts and research progress in physiology and therapy. *Life Med*. 2023;2:lnad013. doi:10.1093/lifemedi/lnad013
31. Zou X, Lei Q, Luo X, et al. Advances in biological functions and applications of apoptotic vesicles. *Cell Commun Signal*. 2023;21:260. doi:10.1186/s12964-023-01251-9
32. Liu H, Liu S, Qiu X, et al. Donor MSCs release apoptotic bodies to improve myocardial infarction via autophagy regulation in recipient cells. *Autophagy*. 2020;16:2140–2155. doi:10.1080/15548627.2020.1717128
33. Zheng C, Sui B, Zhang X, et al. Apoptotic vesicles restore liver macrophage homeostasis to counteract type 2 diabetes. *J Extracell Vesicles*. 2021;10:e12109. doi:10.1002/jev2.12109
34. Lin R, Zhang T, Gao J. Apoptotic vesicles of MSCs: the natural therapeutic agents and bio-vehicles for targeting drug delivery. *Small*. 2023;19:e2301671. doi:10.1002/smll.202301671
35. Huang Z, Zhuang Y, Li W, et al. Apoptotic vesicles are required to repair DNA damage and suppress premature cellular senescence. *J Extracell Vesicles*. 2024;13:e12428. doi:10.1002/jev2.12428
36. Ma L, Chen C, Liu D, et al. Apoptotic extracellular vesicles are metabolized regulators nurturing the skin and hair. *Bioact Mater*. 2023;19:626–641. doi:10.1016/j.bioactmat.2022.04.022
37. Liu D, Kou X, Chen C, et al. Circulating apoptotic bodies maintain mesenchymal stem cell homeostasis and ameliorate osteopenia via transferring multiple cellular factors. *Cell Res*. 2018;28:918–933. doi:10.1038/s41422-018-0070-2
38. Zhou Y, Bao L, Gong S, et al. T cell-derived apoptotic extracellular vesicles hydrolyze cGAMP to alleviate radiation enteritis via surface enzyme ENPP1. *Adv Sci*. 2024;11:e2401634. doi:10.1002/advs.202401634
39. Fei Y, Ling Z, Tong Q, Wang J. Apoptotic extracellular vesicles from supernumerary tooth-derived pulp stem cells transfer COL1A1 to promote angiogenesis via PI3K/Akt/VEGF pathway. *Int J Nanomed*. 2024;19:6811–6828. doi:10.2147/IJN.S466136
40. Ou Q, Huang W, Wang B, et al. Apoptotic vesicles: therapeutic mechanisms and critical issues. *J Dent Res*. 2024;103:1057–1065. doi:10.1177/00220345241265676
41. Medina CB, Mehrotra P, Arandjelovic S, et al. Metabolites released from apoptotic cells act as tissue messengers. *Nature*. 2020;580:130–135. doi:10.1038/s41586-020-2121-3
42. An Y, Geng K, Wang H-Y, et al. Hyperglycemia-induced STING signaling activation leads to aortic endothelial injury in diabetes. *Cell Commun Signal*. 2023;21:365. doi:10.1186/s12964-023-01393-w

43. Liu J, Dou G, Zhao W, et al. Exosomes derived from impaired liver aggravate alveolar bone loss via shuttle of Fasn in type 2 diabetes mellitus. *Bioact Mater*. 2024;33:85–99. doi:10.1016/j.bioactmat.2023.10.022
44. Jiang X, Stockwell BR, Conrad M. Ferroptosis: mechanisms, biology and role in disease. *Nat Rev Mol Cell Biol*. 2021;22:266–282. doi:10.1038/s41580-020-00324-8
45. Ru Q, Li Y, Chen L, Wu Y, Min J, Wang F. Iron homeostasis and ferroptosis in human diseases: mechanisms and therapeutic prospects. *Signal Transduct Target Ther*. 2024;9:271. doi:10.1038/s41392-024-01969-z
46. Buzas EI. The roles of extracellular vesicles in the immune system. *Nat Rev Immunol*. 2023;23:236–250. doi:10.1038/s41577-022-00763-8
47. Mizushima N, Komatsu M. Autophagy: renovation of cells and tissues. *Cell*. 2011;147:728–741. doi:10.1016/j.cell.2011.10.026
48. Li Z, Wu M, Liu S, et al. Apoptotic vesicles activate autophagy in recipient cells to induce angiogenesis and dental pulp regeneration. *Mol Ther*. 2022;30:3193–3208. doi:10.1016/j.ymthe.2022.05.006
49. Qian Z, Wang H, Bai Y, et al. Improving chronic diabetic wound healing through an injectable and self-healing hydrogel with platelet-rich plasma release. *ACS Appl Mater Interfaces*. 2020;12:55659–55674. doi:10.1021/acsami.0c17142
50. Nie W, Huang X, Zhao L, et al. Exosomal miR-17-92 derived from human mesenchymal stem cells promotes wound healing by enhancing angiogenesis and inhibiting endothelial cell ferroptosis. *Tissue Cell*. 2023;83:102124. doi:10.1016/j.tice.2023.102124